A Conceptual Design Study of a Compact Photon Source (CPS) for Jefferson Lab

E. Chudakov,[1] D. Day,[2] P. Degtiarenko,[1] R. Ent,[1] D.J. Hamilton,[3]
T. Horn,[4,1,*] D. Keller,[2] C. Keppel,[1] G. Niculescu,[5]
P. Reid,[6] I. Strakovsky,[7] B. Wojtsekhowski,[1] and J. Zhang[2]

[1] *Jefferson Lab*
[2] *University of Virginia*
[3] *University of Glasgow*
[4] *Catholic University of America*
[5] *James Madison University*
[6] *Saint Mary's University*
[7] *George Washington University*

[*] Contact email:hornt@cua.edu

I Executive Summary

This document describes the technical design concept of a compact, high intensity photon source (CPS) to be used with dynamically nuclear polarized targets to measure processes such as Wide-Angle and Timelike Compton Scattering (WACS and TCS). Capable of producing 10^{12} equivalent photons per second, the deployment of the CPS will result in a large gain in polarized experiment figure-of-merit (by a factor of $\sim$30). Compared to a traditional bremsstrahlung photon source the proposed solution will present several advantages, including much lower radiation levels, both prompt and post-operational due to the beam line elements radio-activation. For use with polarized targets, the heat load and radiation damage effects are well within the acceptable range. The design is flexible allowing the CPS to be converted into a K_L beam for spectroscopy experiments.

PAC43-PAC45 at Jefferson Lab saw several proposals and LOIs which require the CPS. One of these is C12-17-008 (Polarization observables in Wide-angle Compton scattering at large s, t, and u), which was conditionally approved subject to a technical review. The issues in the PAC45 report to be addressed are: to finalize the design and price estimate for the CPS, and to clearly establish the expected maximum photon intensity. **The goal of this document is to address the PAC45 technical comments for full approval of C12-17-008.**

The CPS final design features a magnet, a central copper absorber, and hermetic shielding consisting of tungsten powder and borated plastic. The addition of the latter has a considerable impact on reducing the neutron flux escaping the CPS. The ultimate goal in this design process is that radiation from the source should be a few times less than from a photon beam interacting with the material of a polarized target. The equivalent heat load for a pure photon beam impinging such targets corresponds to a photon flux originating from a 2.7 μA electron beam current striking a 10% copper radiator. Detailed simulations of the power density and heat flow analysis show that the maximum temperature in the absorber is below 400 degrees, which is well within the acceptable range of copper, and thus demonstrates that the CPS can absorb 30 kW in total (corresponding to 11 GeV beam energy and 2.7 μA beam current).

The CPS fulfills the requirements on operational dose rates at Jefferson Lab, which has been established with extensive and realistic simulations. The projected prompt dose rate at the site boundary is less than 1 μrem/hr (to be compared with 2.4 μrem/hr, which corresponds to a typical JLab experiment that does not require extra shielding). The activation dose outside the device envelope at one foot distance is less than several mrem/hr after one hour following the end of a 1000 hour run ($\sim$ 40 PAC days). The activation dose at the pivot in the experimental target area, where operational maintenance tasks may be required, is dominated by the dose induced by the pure photon beam. At a distance of one foot from the scattering chamber it is less than several mrem/hr one hour after the end of a 1000 hour run (i.e. the additional activation dose induced by absorption of the electron beam in the Compact Photon Source is negligible).

This document demonstrates that the CPS with an optimized shielding design provides a photon flux of 1.5×10^{12} equivalent photons/s, with a factor of 1000 reduction in prompt radiation dose compared to a 2.7 μA (30 kW) electron beam current striking a 10% copper radiator. The CPS meets the acceptable radiation level requirements for a typical run time of 1000 hours

with the photon source located at 2-3m from the target. The technical design and installation in the existing hall infrastructure is feasible. The estimated cost is on the order of $4M and is dominated by the raw material costs of tungsten.

This document is organized as follows. In section II, we outline the science gain with CPS in combination with dynamically nuclear polarized targets including the use of an effective rastering of the beam at these high intensities. The heat load and power deposition are also discussed. In section III, the conceptual design and component details of the CPS are presented. Section IV lists the requirements a CPS has to meet to fulfill operational dose rates at Jefferson Lab. In section V, we discuss the results of our shielding design and optimization studies and compare them with the requirements in section IV. Finally, section VI deals with engineering and safety aspects including material considerations, installation, and a preliminary cost analysis. Appendix 1 describes the CPS concept transfer to Hall D. Appendix 2 includes a benchmark comparison of the different simulations used in our shielding design studies.

II Motivation: Science Gain with CPS

A Polarization Observables in Wide-Angle Compton Scattering

Investigating the three-dimensional structure of the nucleon has been an active and productive field of research especially during the last two decades since the invention of the GPD formalism, and continues to be central to the hadron physics program at JLab. The GPD formalism provides a unified description of several important reactions such as elastic electron scattering, DIS, DVCS/TCS, WACS and meson production, which can all be described by a single set of four functions H, $\tilde{H}$, E and $\tilde{E}$. These functions need to be modeled and constrained with parameters extracted from experimental data. The WACS experimental observables provide several constraints for GPDs which are complementary to other exclusive reactions due to an e_a^2 factor and an additional $1/x$ weighting in the GPD integrals for WACS. For example, the elastic form factor $F_1(t) = \sum_a e_a \int dx H^a(x,0,t)$ is related to the WACS vector form factor $R_V(t) = \sum_a e_a^2 \int \frac{dx}{x} H^a(x,0,t)$, both of which are based on the same underlying GPD $H(x,0,t)$. Similarly, polarized observables in WACS uniquely provide high $-t$ constraints on $\tilde{H}(x,\xi,t)$ via extraction of the WACS axial form factor $R_A(t)$ in a kinematic regime where precise data on the nucleon axial form factor is not available.

Polarized WACS experiments need to be performed at large photon energy and scattering angle where the assumption of a factorized reaction amplitude is valid and the GPD-based calculations are reliable ($s, |t|, |u| > 2.5$ GeV^2). The experimental challenges associated with double-polarization measurements of photon-induced reactions at high momentum transfer are formidable. Detector rate capabilities and radiation hardness are both severely tested in beam-recoil measurements as a result of a rapid decrease in recoil proton polarimeter analyzing power at high $-t$. Utilization of a mixed electron-photon bremsstrahlung beam, on the other hand, limits luminosity in beam-target measurements

due to loss of target polarization, primarily as a result of electron-induced heat load. In the preparation of a 12 GeV Jefferson Lab experimental proposal (C12-17-008) on polarized wide-angle Compton Scattering (WACS), a completely new experimental approach was developed, based on deploying a high-intensity compact photon beam source and a polarized target. This new technique opens up physics possibilities that had hitherto been inaccessible at tagged photon facilities and results in a significantly improved figure-of-merit (of a factor of ∼30) over all previous double-polarization measurements involving photon-induced reactions.

B Compatibility with Polarized Targets

Target System and Required Modifications

The WACS experiment will use a polarized proton target developed by UVa/JLab, which has typically been exposed to a beam of 100 nA electrons and provided a run-averaged proton polarization of approximately 70%. The beam must be moved over the 25 mm face of the target cup to ensure that the target material is exposed uniformly to the depolarizing effects of the beam. If the beam were to remain at one location for an extended period it would drill a 'hole' in the target where the polarization has fallen due to local heating and radiation damage. As the NMR system samples the entire target it would, in this case, indicate a much larger value than that where the scattering was taking place. Rastering the beam across the face of the target continuously removes this problem and was made possible in the past by the combination of the standard hall fast raster of ±2 mm and a specially constructed slow raster. However, as discussed in the next section the proposed Compact Photon Source has a very small exit aperture of 3 mm by 3 mm, limiting possible beam motion.

An alternative approach for the beam-target raster is found in Ref. [1] and includes a combination of the target rotation around the horizontal axis and ±10 mm vertical motion of the target ladder. Such a raster method effectively moves the motion complexity out of the high radiation area of the absorber. Here we layout the requirements for the rotation and vertical motion which will provide the same uniform exposure as the electron beam raster system used up to now. We start from the premise that the target system with the CPS will be able to handle the the same heat load from the photon beam and the microwave source as used in electron beam experiments. From the perspective of low energy production of free radicals in the target material, this approximation is expected to be good within 10%. However the free radical complex produced from a high energy beam ($E_{beam} > 20$ MeV) and the way these radicals can effect the polarization is not yet well understood. For now we focus only on the ionization energy loss produced by the multi-GeV photon beam as e^+/e^- pairs. The energy loss from these processes is approximately independent of beam energy and is estimated to be about 2 MeV g^{-1} cm^2.

For a photon intensity of 1.5×10^{12} equivalent photons per second it is necessary to use an evaporation refrigerator with ∼1 Watt cooling power in combination with a high polarization, high radiation resistant proton target material (NH_3). For electron beam experiments typically 100 nA is the maximum current on the target. The heat load in a

3 cm long target can be calculated for NH_3 with density 0.917 g/cm^3 leading to,

$$2[\mathrm{MeVcm}^2/\mathrm{g}](1.6\times10^{-13}[\mathrm{J/MeV}])6.25\times10^{11}[\mathrm{s}^-1](3[\mathrm{cm}])(0.917[\mathrm{g/cm}^3]).$$

Considering the target packing fraction, only about 60% of the ionization energy is actually deposited into the target, leading to about 0.33 Watts. Combined with the heat deposit from microwaves (0.5 W) used to dynamically polarize the target, the cooling power of the UVA/JLab evaporation fridge and pumping system is not saturated. However, cooling power is not the only concern. This heat load must be distributed throughout the target so that the target material beads are not over-heated on the material boundary so as to create local depolarization. To do this with electrons a beam rastering system can be used to distribute the beam over the surface of the target face. The slow raster that spirals out is combined with the faster raster system which distributes the beam in a 2 mm^2 square pattern. The CPS is designed to utilize the fast raster system – however without some sort of slow rastering there would be significant depolarization in the region around the photon beam spot due to material interfacial thermal heating (ITH).

The ionizing radiation inside the target is the primary source of the NH_2 free radicals and the ITH. Using simulations with the previously mentioned photon flux and a 2 mm^2 beam profile leads to 25 nA of ionizing radiation at the exit of the target in an area of about 6 mm^2 (containing 90% of the ionizing particles). Taking this spatial distribution to hold the full 0.33 W heat load from the high intensity photon beam implies that about 100 target beads with an average radius of 1 mm hold all the heat. To calculate the effects of this heat load on the local polarization we must first start with the heat equation for a volumetric heat source. This can be expressed as,

$$C_{p0}T^3\rho\frac{dT}{dt} = \dot{Q} - 3R_\alpha\frac{T^4 - T_B^4}{r_{bead}}. \tag{1}$$

Using the corresponding values, this equation can be solved with the initial condition $T(0) = 1K$. $\dot{Q}$ is the volumetric heat load per bead which is conservatively estimated to be 0.72 W/cm^3. Using the specific heat for NH_3 of $C_{p0} = 8.8\times10^{-6}$ J g^{-1} K^{-4}, with ammonia Kapitza conductance $R_\alpha = 1.43\times10^{-2}$ W cm^{-2} K^{-4}, with T_B as the liquid helium bath temperature (1 K), and T is the dynamic material boundary temperature. The solution to this relation gives the boundary temperature as a function of time and is shown in Figure 1.

These results indicates that after a few microseconds the surface of the bead increases by about 0.25 K. We can then estimate the time it takes to heat the bead all the way through from the heat on the surface assuming spatial uniformity,

$$\Delta t = \frac{\rho V C_p \Delta T}{\dot{Q}}. \tag{2}$$

This calculation results in a time of just a few μs to heat the entire bead from the outer surface. These times are small on the scale of the time it take for the polarization to change. To estimate the time it takes to drive the polarization down from the material beam heating we must consider the DNP rate parameters of NH_3. This decay time is related to the microwave power and the spin-lattice relaxation rate. The equations of motion that give the rate of depolarization can be approximated using the form,

$$\frac{dP(t)}{dt} = \beta T^4(P_{lim} - P(t)). \tag{3}$$

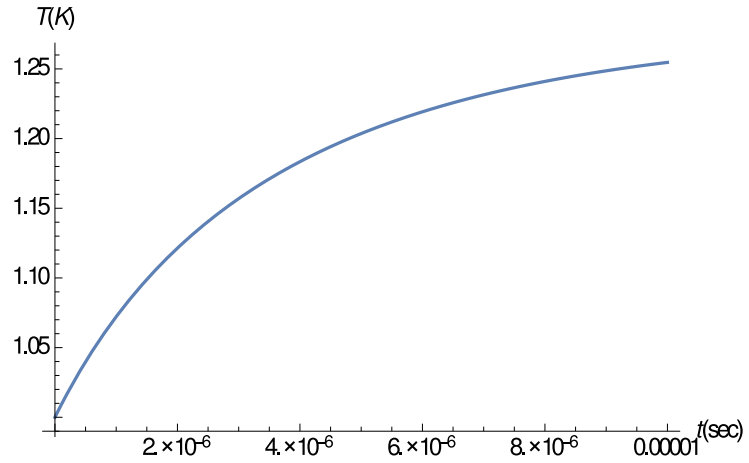

Figure 1. Ammonia bead temperature rise due to the beam heat load.

The polarization, limited by the new thermal conditions from Eq. 3, is contained in P_{lim}, which is an estimate based on the Brillouin function. The parameter β contains the rate information and comes from polarization data. The starting polarization of 93% is used as an example. Solving Eq. 3 numerically results in an approximation of the polarization drop over time. It is worth noting that calculations here are only estimates and several necessary parameters required have considerable uncertainty. We use the results as only a guide to give an order of magnitude check on the time needed to rotate the target cell. Figure 2 indicates that the beads should only stay within the same position in the ionizing shower for no more than a few seconds or the polarization will decrease. This change would not register in the NMR signal. A rotation on the order of once every few seconds is adequate for this purpose.

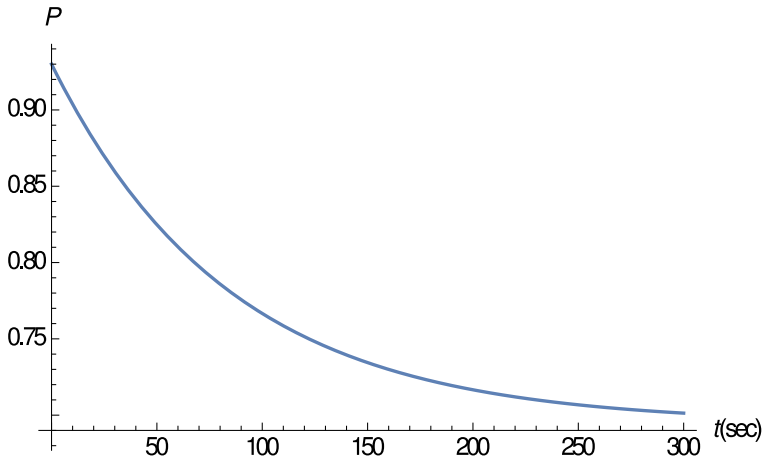

Figure 2. Target polarization as a function of time for beads within the ionizing shower.

1 Design of Rotating Target

In order to increase the area of the target that the photon beam will interact with a rotating target was developed to raster photons over the target cup face, see Figure 3. The Kel-F target cup is machined to include a gear that can be driven from a rotating shaft along the target insert. Figure 3 shows a design of the same dimension of polarized targets used in the past (2.5 cm diameter by 3 cm length) that fit within the homogeneous field region of the polarizing 5 T magnet. In the design shown there is no additional material

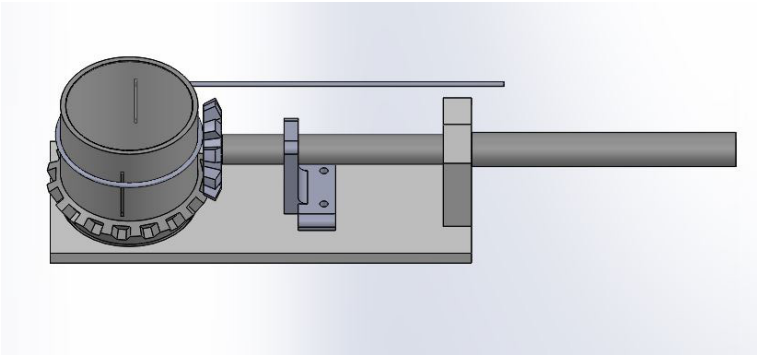

Figure 3. The rotating target cup driven by a gear and shaft with the NMR loop around the target cell.

from the cup in the beam-line. The front and back of the target cell are made of a thin aluminum foil (not seen in the diagram). The rotation is driven by a gear and shaft. The NMR couples inductively to the target material by a coil wound around outside of the cup. The rotating shaft passes through the top of the target insert using a vacuum rotary feed-through which is then driven by a electric motor.

The target rotation in combination with the standard target actuator results in an effective slow raster which spirals over the full area of the standard 2.5 cm diameter target. The beam collimation provides the spot size on the target and couples directly to the resolution characteristics for reconstruction at the cost of holding the beam location in space fixed. We can still obtain uniform exposure of the target cell by a combined rotation of the target cup synchronized with an up/down movement of the target ladder. Rotation of the target cup has already proven viable in many UVA tests. Depolarization and homogeneous radiation damage can easily be achieved by continuously moving the target at a rate determined by the radius of the circle made through rotation on the target surface, spending no more than a few hundred milliseconds on each target location. So even near the center only 0.01 Hz is required. To avoid mechanical vibration that can induce noise in the NMR signal it is possible to make several rotations in a fixed diameter before moving to the next actuator position. This reduces the up and down motion required to cover the same area. At UVA rotation rates of several Hz have already been demonstrated. By completing a fixed number of rotations for each experimental run, false asymmetries and fluctuations from the variations in target bead packing can be averaged out.

III The Compact Photon Source

A Conceptual Design

A traditional source of bremsstrahlung photons includes a radiator, a deflection magnet and a beam dump for the undeflected electrons, augmented for energy-tagged photon beams with a set of focal plane detectors covering a modest to large momentum acceptance. Such a configuration requires significant space along the beam direction and heavy shielding around the magnet and the beam dump, which have large openings due to the large angular and energy spread of the electrons after interaction with the radiator. In addition, without tight collimation the traditional scheme leads to a large size of the photon beam at the target due to divergence of the photon beam and the long path from the radiator to the target. The beam spot size contributes to the angular and momentum reconstruction resolution of the resultant reaction products due to uncertainty in the transverse vertex position. Lastly, it is often associated with producing appreciable radiation doses, as particles are allowed to propagate over short distances before mitigation of radiation by containment starts to be effective.

A new solution for a photon source was proposed in a report at the NPS collaboration meeting in November 2014 about a new experiment for a double polarized WACS (see a detailed analysis of the CPS in Ref. [2]). Reconstruction of the scattered photon in WACS depends on multiple factors including the photon beam spot size at the target, for which the distance from the radiator to the target is the most important factor. Dedicated studies prepared prior to the WACS proposal submission have shown that a spot size of around 2 mm is well matched to preserve the benefits of the proton arm angular resolution and the spatial resolution of the photon arm [3].

The concept of a new source takes advantage of the narrowness of the photon beam relative to the angular distribution of the secondary particles produced in the electron-nuclei shower. Indeed, the photon beam angular spread, dominated by electron multiple scattering in the $10\%X_o$ radiator, is about $4/E_{beam}$[MeV]$\sim$0.4 mrad, but the secondary particles survived filtering through a one nuclear interaction length ($\sim$140-190 g/cm^2 or $\sim$15 cm) of the heavy absorber, have an angular spread of 100-1000 mrad.

The main elements of the CPS are shown in Figure 4. Without loss of photon intensity, a channel (a collimator for the secondary radiation but not for the photon beam) around the photon beam could be as narrow as the photon beam size with natural divergence plus the size of the beam raster. After passing through the radiator, the electron beam should be removed from the photon line by means of a magnet. The length, aperture and field of the magnet are very different in the proposed source from the traditional one. In the traditional source the magnet is needed to direct the electrons to the dump. Because of the large momentum spread of electrons which have interacted in the radiator, the magnet aperture needs to be big and the dump entrance should be even bigger: 13% of the beam power would be lost before the beam dump, even with a 10% momentum acceptance of the beam line. In contrast, in the proposed source the magnet acts as dump for the electrons with a cone of photons escaping through a small collimator.

The electron energy dumping starts on the side of the photon beam channel, so a

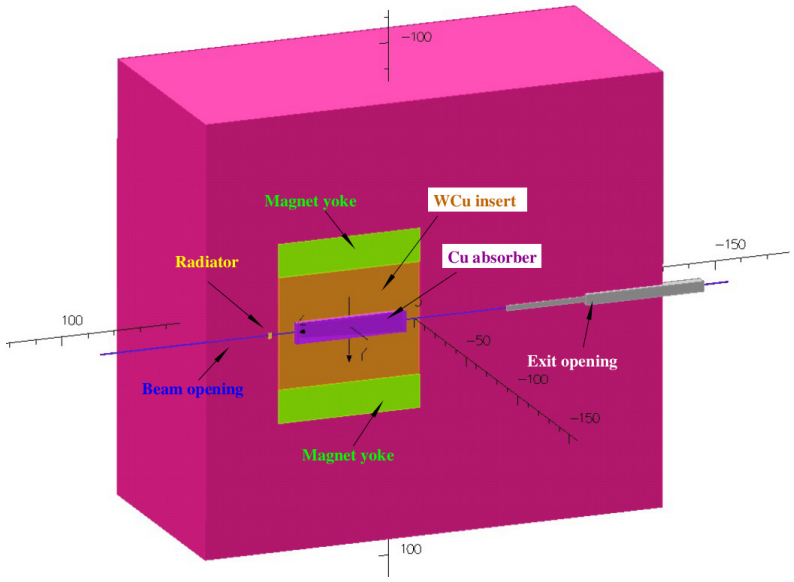

Figure 4. The CPS cut-off view. Most of the deflected electrons strike a copper absorber, surrounded by a W-Cu insert inside the magnet yoke. The outer rectangular region in this view is the tungsten-powder shield.

shift of the electron trajectory by just 1-3 mm is already sufficient for the start of the shower. At the same time, such a deflection needs to be accomplished at a relatively short distance (much shorter than the size of the radiation shielding) after the beam passes through the radiator to keep the source compact. Indeed, with a deflection radius, R, a vertical size of the channel, $2a$, and a vertical raster size, $2b$, the trajectory enters the channel side after traveling in the magnetic field a distance, p, which varies from $p = \sqrt{2\,R\,(a-b)}$ to $p = \sqrt{2\,R\,(a+b)}$ (see the scheme in Figure 5). In the currently

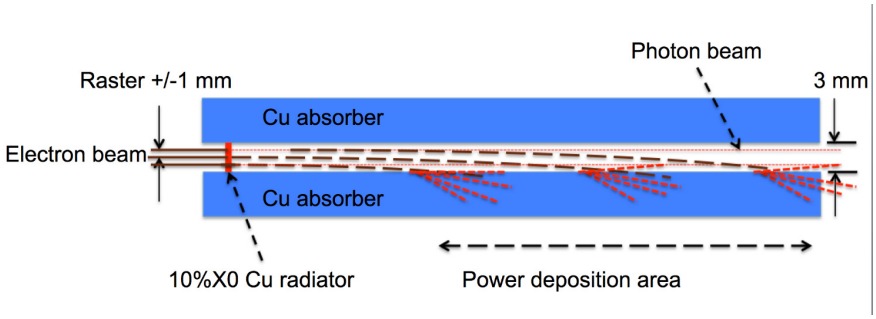

Figure 5. The scheme of beam deflection to the absorber/dump.

proposed CPS magnet the trajectory radius R is about 10 m for 11 GeV electrons, the channel size is 0.3 cm, and the raster size is 0.2 cm, so the distance p has an average value of 17 cm with a spread of 12 cm. A total field integral of 1000 kG-cm is adequate for our case, which requires a 50 cm long iron dominated magnet.

The above concept of the combined magnet-dump allows us to reduce dramatically

the magnet aperture and length, as well as the weight of the radiation shield, due to the compactness of the source and minimization of openings, thus significantly reducing the radiation leakage. Such a conceptual design opens a practical way forward for a CPS, providing one can manage both the radiation environment in the magnet and the power deposition density in the copper absorber.

B Magnet

Normal conducting magnets for operation in high levels of radiation have been constructed at several hadron facilities, including the neutron spallation source at ORNL and the proton complex JPARC. We designed the magnet with permendur poles tapered in two dimensions, which allows us to reach a strong magnetic field at the upstream end of the magnet (3.2 Tesla), with the coils located 20 cm from the source of radiation. The resulting radiation level at the coil location is calculated to be low enough, below 1 Mrem/hr, to allow the use of a modest-cost kapton tape based insulation of the coils. The length of the magnet was selected to be 50 cm and the field integral 1000 kG-cm. Figure 6 shows the longitudinal profile of the magnetic field obtained from OPERA calculations.

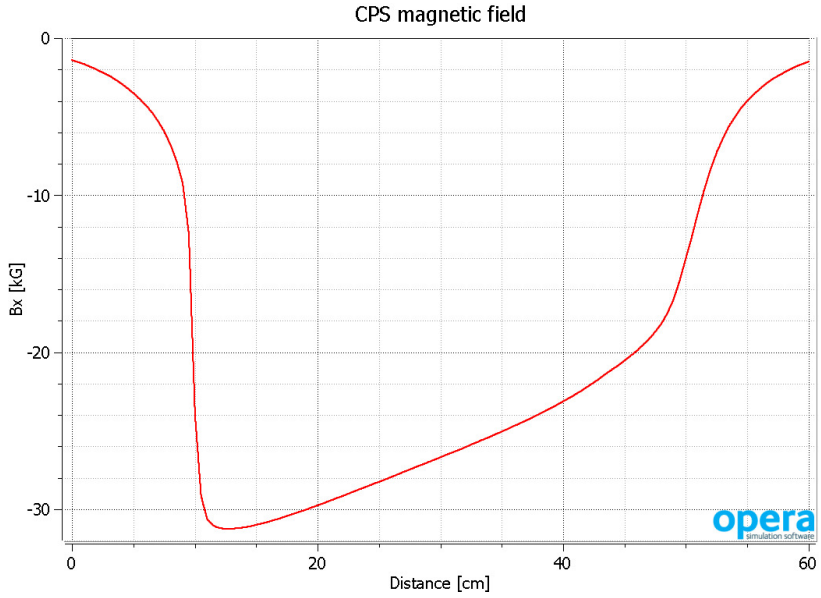

Figure 6. Magnetic field (B_x) profile along the beam direction, as a distance from the radiator position.

C Central Absorber

The beam power is deposited in an absorber made of copper, whose high heat conductivity helps to manage the power density. An absorber made of aluminum would help to reduce power density by a factor of 2-3 compared with copper due to its smaller radiation length, but it would also increase the length of the CPS by about 50 cm so

is not preferred. The heat removal from the copper absorber is arranged first via heat conductivity to the wider area where water cooling tubes are located. Figure 7 shows the longitudinal profil

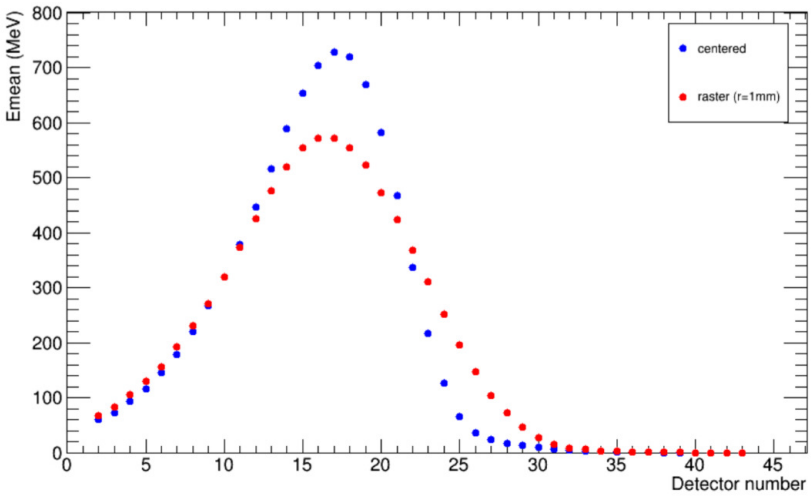

Figure 7. Longitudinal profile of the energy distribution (integrated for one cm copper slab) for a single 11 GeV incident electron. The maximum power density is occurs at a distance of 18 cm from the radiator. The blue dots show the energy deposition for the electron beam centered in a 3 mm by 3 mm channel. The red dots show the same for the beam rastered with a radius of one mm.

The transverse distribution of power is also very important to take into account because, for a high energy incident beam, it has a narrow peak. A detailed MC simulation of the deposited power density and the 2-dimensional heat flow analysis were performed to evaluate the maximum temperature in the copper absorber. Figure 8 (left panel) shows the layout of materials in the model used for the temperature analysis. The calculation was performed for the case of a 11 GeV 30 kW beam and a 10% X0 radiator, and the temperature was found to be below 400°C, which is well in the acceptable range for copper. Figure 8 (right panel) shows the temperature profile in the transverse plane at the longitudinal location of maximum power deposition. Cooling of the core will require about four gallons of water per minute at 110 psi pressure (at 30°C temperature rise), which is easy to provide.

D Tungsten-powder Shield

The amount of material needed for radiation shielding is primarily defined by the neutron attenuation length, which is 30 g/cm^2 for neutrons with energy below 20 MeV and 125 g/cm^2 for high energy neutrons. The neutron production rate by an electron beam in copper is 1×10^{12} per kW of beam power according to a SLAC report (W.P. Swanson, SLAC-PUB 2042, 1977, see Figure 9). At a distance of 16 meters from the unshielded source for a 30 kW beam, the neutron flux would be 1×10^7 n/cm^2/s, which would produce a radiation level of 110 rem/hr, or 850 times higher than during the RCS

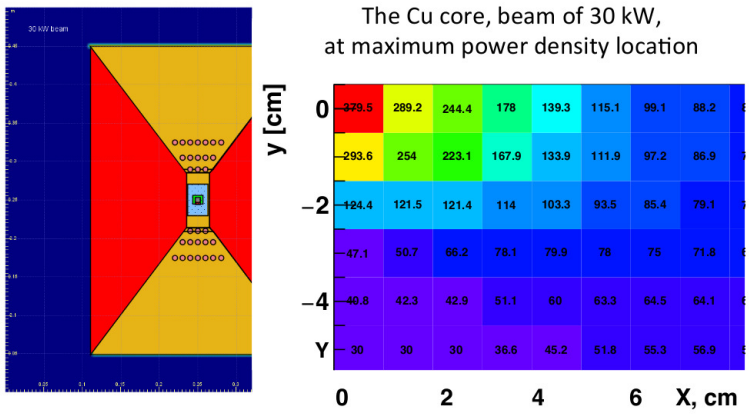

Figure 8. Left panel: the cross section of the absorber (shown in blue (copper) in the center and yellow (W-Cu(20%)) surrounding) with the water cooling channels. Right panel: the temperature map for 1 cm by 1 cm elements at the longitudinal coordinate of the power deposition maximum.

experiment at JLab (E99-114) (at a 16-meter distance from the pivot in the upstream direction). The current conceptual design with a total shield mass of 850 g/cm^2 will result in reduction in these radiation levels by a factor of 1000.

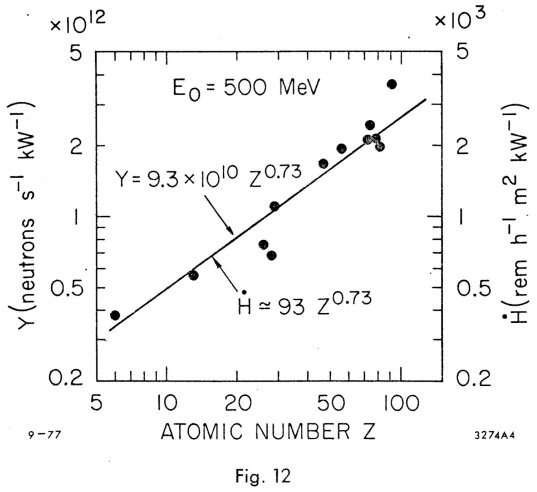

Fig. 12

Figure 9. The neutron yield according to SLAC-PUB 2042.

The space inside the magnet between the poles and coils is filled by an inner copper absorber and an outer W-Cu(20%) insert, which provides a good balance between effective beam power absorption and radiation shielding. For the shield outside the magnet, the current design uses tungsten powder, whose high density (16.3 g/cm^3) helps to reduce the total weight of the device. A thickness of 50 cm was used as a first iteration for the thickness of the outer shield of the CPS, but we have investigated the impact of varying this amount of outer shielding (as discussed later in the document).

E Impact on Polarized Target

The most significant gain associated with deployment of the CPS is for experiments using dynamically polarized targets. However, such polarized targets operate with strong 2.5-5 Tesla polarizing fields themselves. In addition, dynamically polarized target operation imposes strict requirements on the field quality at the target location, where fields and gradients need to be compensated at the 10^{-4} level. This necessitates studies of the mutual forces associated with the 2-3 Tesla CPS dipole magnet and the 5 Tesla polarized target solenoid, in terms of both the design of the support structures and the operation of the polarized target.

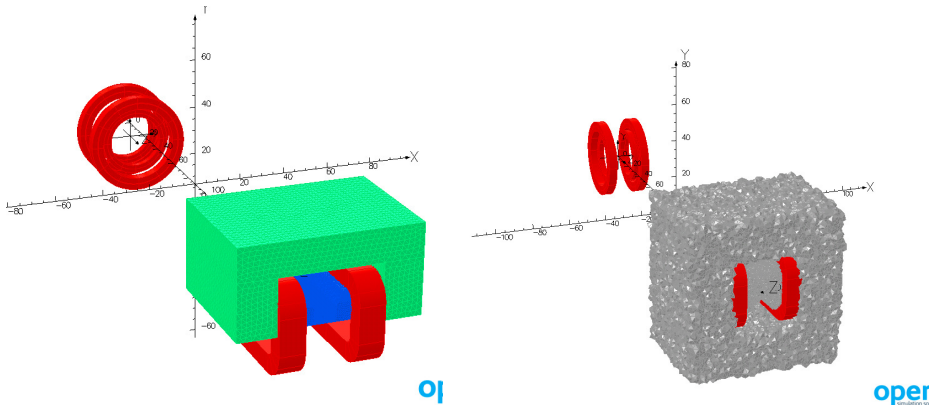

Figure 10. The TOSCA model used in the field and force calculations, for longitudinal orientattion of the coils/target polarization (left) and transverse orientation (right).

The fields associated with the combination of these two magnetic systems were calculated using the model shown in Figure 10 (left panel, for the polarized target configured for longitudinal polarization), with the following results obtained:

- When the CPS is ON but the polarized target magnet is OFF, the (total) field at the target location amounts to only about 0.1 Gauss.
- When the polarized target magnet is on and the CPS is OFF or removed, the field at the CPS location is about 130 Gauss.
- When both the CPS is ON and the polarized target magnet is ON, the field gradient at the polarized target center is about 2 Gauss/cm (Figure 11).

These results show that, for the CPS the induced field is mainly due to the CPS magnet yoke becoming polarized by the target field. Whereas for the target, the field gradient at the target location is sufficiently low for routine dynamically polarized NH_3 or ND_3 target operation, with a relative values of 0.4×10^{-4}.

The forces between the polarized target and CPS magnets were calculated by using several methods, including an analytical estimate for the 700 kA per coil (four of them in the target) and the observed field gradients. The gradients lead to about a 20-30 Gauss difference in B_x, B_y at the locations of the two sets of coils (transverse to the beam direction). The force F_z (along the beam line) was found to be about 200 N, which is well

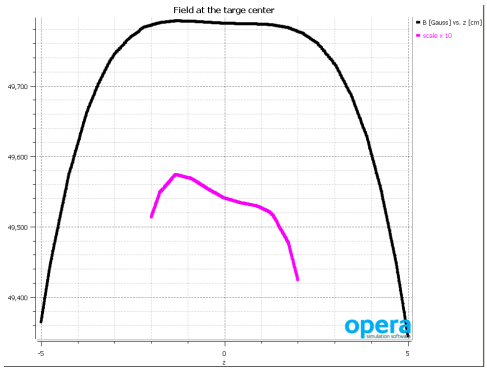

Figure 11. The field at the target center. Insert shows a field zoomed by a factor of 10. Values of the field (B) in Gauss and the coordinate (z) in cm.

below the recommended limit of 1000 N. This is the value that should be considered for support structure engineering designs. A similar force analysis for the polarized target magnet configured in a *transverse* (horizontal) orientation of the target field (see Figure 10 (right panel)) shows that the resulting force is slightly lower and the gradient at the target (B_x in this case) is around the same 2 Gauss/cm value.

IV Radiation Requirements

As discussed previously, the WACS experiment with the proposed CPS will utilize a dynamically nuclear polarized target. Electron beam currents for use with such targets are typically limited to 100 nA or less, to reduce both heat load and radiation damage effects. The equivalent heat load for a pure photon beam impinging on such a target corresponds to a photon flux originating from a 2.7 μA electron beam current striking a 10% copper radiator. The radiation calculations presented in this section therefore assume a CPS able to absorb 30 kW in total (corresponding to a beam of 11 GeV electrons with a current of 2.7 μA). In addition, the beam time assumed for a typical CPS experiment is 1000 hours ($\sim$40 PAC days).

For such an experiment, the following radiation requirements must be fulfilled:

- The prompt dose rate in the experimental hall must be $\leq$ several rem/hr at a distance of 30 feet from the CPS.
- The prompt dose rate at the site boundary must be ≤ 1 μrem/hr. (For comparison, 2.4 μrem/hr is the corresponding rate for a typical Jefferson Lab experiment which does not require extra shielding).
- The activation dose outside the CPS envelope at a distance of one foot must be $\leq$ several mrem/hr one hour after the end of a 1000 hour run.
- The activation dose at the pivot in the experimental target area, where operational maintenance tasks may be required, is dominated by the dose induced by a pure photon beam, and at a distance of one foot from the scattering chamber must be $\leq$

several mrem/hr one hour after the end of a 1000 hour run (i.e. the additional dose induced by radiation of the main beam absorbed in the CPS should be negligible).

The CPS design should combine in a single shielded assembly all elements necessary for the production of the intense photon beam and ensure that the operational radiation dose rates are within the requirements outlined above. Much of this is achieved by keeping the overall dimensions of the CPS as small as possible, by careful choice of materials, and by locating radiation shielding as close to the source of radiation as possible. Compared to a traditional bremsstrahlung photon source, the proposed solution will present several advantages, including much lower radiation levels, both prompt and post-operational due to the beam line elements radio-activation, as will be shown later in this section.

The CPS conceptual design has been established with extensive and realistic simulations. As validation of the simulation tools used, benchmark comparisons were made with GEANT3, GEANT4, FLUKA and DINREG. The benchmark results are further described in Appendix 2. After benchmark validation, an extensive series of radiation calculations were performed in order to:

- Determine the size and layout of the shielding around the magnet, and the choice of materials (copper, Cu-W alloy, concrete, borated plastic, etc.).
- Determine the magnet field requirements in terms of peak field, gap size, and field length.
- Determine the radiation levels on the magnet coils, and based on these results to identify radiation hardened materials that might be used in building the coils.
- Determine the radiation levels on the polarized target electronics.
- Determine the radiation levels directly adjacent to the CPS as well as at the experimental hall boundary.

The logic behind the CPS hermetic shielding design is that radiation (γ, n) from the source should be a few times less than from a photon beam interacting with the material of a polarized target. The CPS is designed to meet the radiation level requirements specified in Appendix 2 for an electron beam current of 2.7μA (30 kW), run time of 1000 hours, and the photon source as close to the target as possible. The shielding design consists of tungsten powder and 10 cm of 30% borated plastic. The addition of the latter has considerable impact in reducing the neutron flux escaping the CPS, illustrated in Figure 15.

V Radiation Studies and Shielding Design

In this section we will describe several different configurations for comparison, the first of which is the default situation for dynamically nuclear polarized targets in Hall C and elsewhere, which is that of a 100 nA incident electron beam. The second configuration corresponds to the equivalent photon flux created by a 2.7 μA electron beam on a 10% copper radiator incident on the same polarized target system. In this scenario, we remove

all the secondary particles generated in order that it mimics a pure and background-free photon beam. The third scenario is one with the CPS under the same conditions, a 2.7 μA electron beam on a 10% copper radiator, for which all the radiation background is included in the simulation. In some cases we have simulated only the effect of the CPS, while in others the CPS and the target system combined are considered.

A Prompt Radiation Dose without a Target

In order to help introduce the shielding concept of the CPS, we start by comparing the prompt radiation doses as calculated in a ring detector covering a radial range between 5 and 10 cm from the beam line. We first calculate the prompt dose originating from a 2.7 μA electron beam hitting a 10% copper radiator a distance of 2.15 m upstream of the pivot. There is no target system in this simulation, which means that all prompt radiation originates from the interaction between the primary beam and the radiator. Figure 12 shows two-dimensional dose rates originating from photons only (top left), from neutrons only (top right), from all particles (bottom left), and the one-dimensional prompt radiation dose along the beam direction (bottom right). Obviously, except for the neutron contribution most of the prompt radiation is created along the beam direction. The prompt radiation levels reach roughly 40 rem/hr, of which only around 200 mrem/hr is in the form of gamma radiation and 10 mrem/hr from neutrons. The remaining and clearly dominant contribution are the charged electrons and positrons created, inducing further showers.

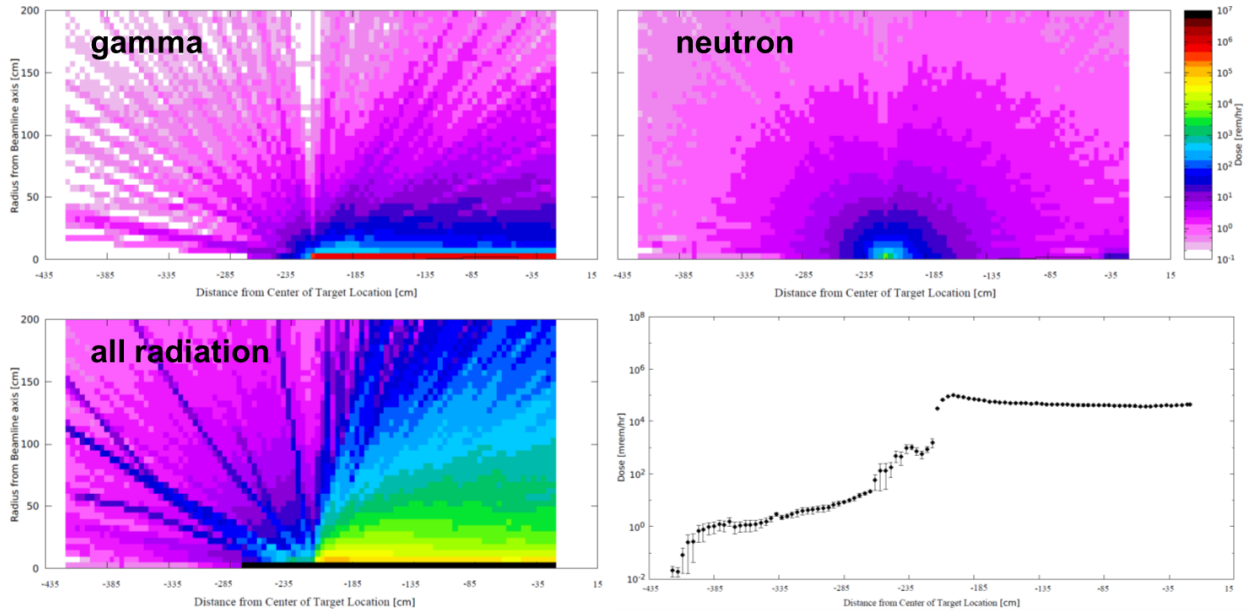

Figure 12. Two-dimensional dose rates as originating from photons only (top left), from neutrons only (top right), from all particles (bottom left) and the (one-dimensional) prompt radiation dose along the beam direction (bottom right).

A striking difference is observed in the case of a 2.7 μA electron beam incident on

a 10% copper radiator as before, but now located within the CPS. Figure 13 illustrates the prompt radiation dose along the beam direction. The y-axis scale on this figure is the same as in Figure 12 (bottom right panel). One can therefore clearly see that the prompt radiation (again, in a 5 to 10 cm ring detector along the beam axis) within the CPS is much higher (300 times, because with CPS the full power of the beam is deposited). Crucially, however, the prompt radiation dose outside the CPS is reduced by a factor of over 1000 to roughly 15 mrem/hr. This factor is entirely consistent with the reduction factor of estimated previously in section III D.

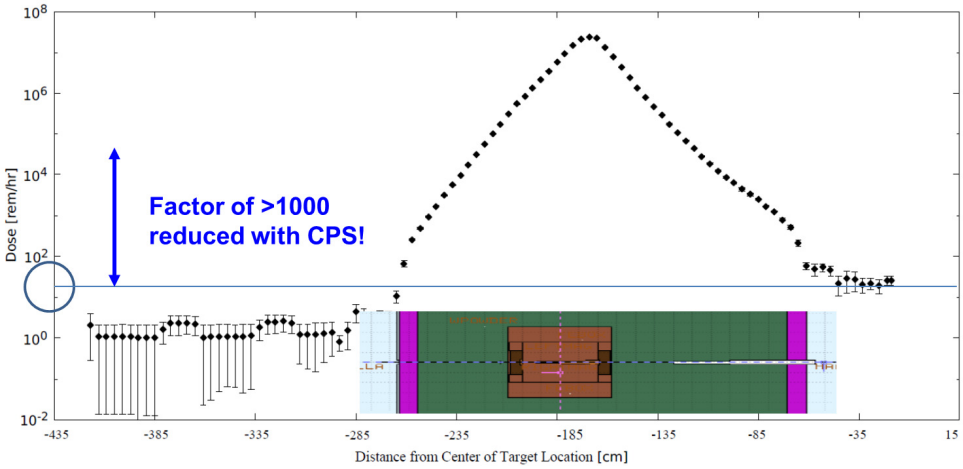

Figure 13. One-dimensional prompt radiation dose along the beam direction, from all particles. The large reduction factor of >1000 induced by the Compact Photon Source design outside the magnet itself is apparent. Along the beam line inside the magnet, the prompt radiation dose can go up to above 10 Mrem/hr, dropping rapidly with distance.

This extremely important result is further illustrated in Figure 14. In stark contrast with the case without the CPS, there is now no contribution to the prompt dose from photons, electrons and positrons – the neutron-only dose rate is nearly identical to the all-radiation rate. The fourth panel in Figure 14 (bottom right) illustrates how well an optimized CPS shielding concept absorbs the prompt radiation. Outside the CPS the prompt radiation dose rate on the surface (indicated by the outer black rectangular lines) is reduced to a maximum level of roughly 10 rem/hr. This shielding concept is so effective because of the fact that the development of showers generated by interactions of the primary beam is highly suppressed and the resultant secondary particles contained. This confirms that with a CPS the following requirement can be met: **prompt dose rate in hall $\leq$ several rem/hr at 30 feet from device**.

B Impact of Boron and Shielding Optimization

It is well-known that the neutron flux through a surface can be drastically reduced by the addition of boron as a result of the very high capture cross section of ^{10}B. We simulated this effect by calculating the neutron flux at the CPS boundary assuming various thicknesses of tungsten shielding (65, 75 and 85 cm radial), and then adding 10 cm of

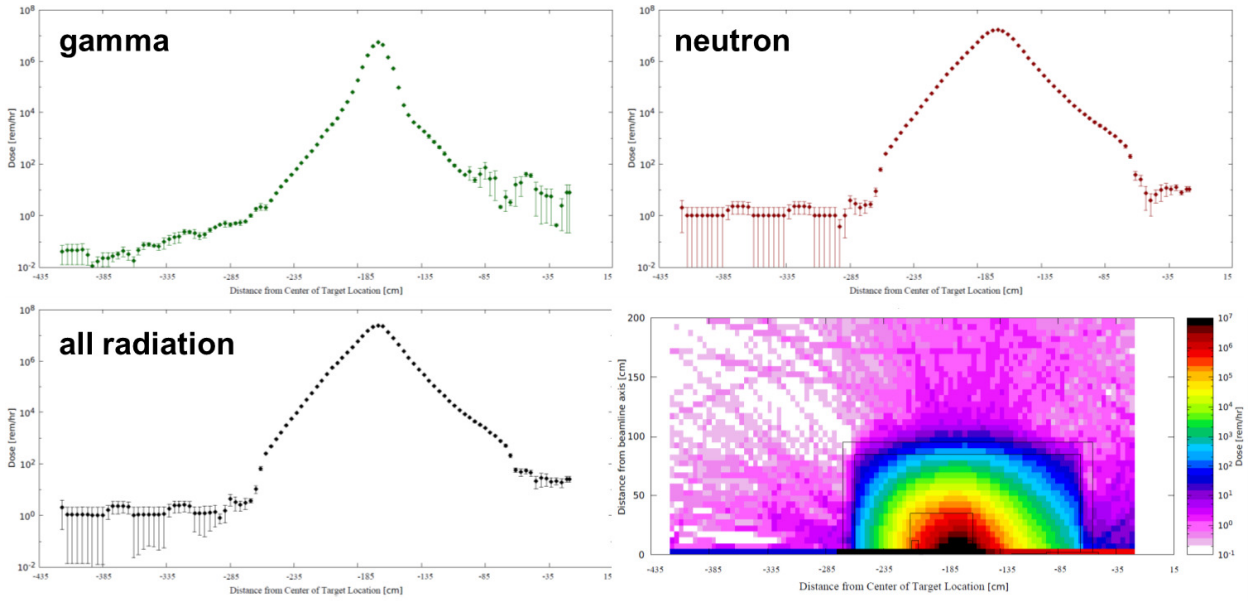

Figure 14. The (one-dimensional) prompt radiation rates as originating from photons only (top left), from neutrons only (top right), and from all radiation sources (bottom left). The fourth panel (bottom right) illustrates how well an optimized CPS shielding concept absorbs the prompt radiation, outside the CPS the prompt radiation is on the surface (indicated by the outer black rectangular lines) already reduced to a level of roughly 10 rem/hour at most.

borated (30%) plastic. The result can be seen in Figure 15, which shows the neutron flux as function of neutron energy (on a logarithmic scale). Adding 10 cm of tungsten clearly reduces the neutron flux as expected, but a much more drastic reduction is seen when the 10 cm of borated plastic is added. Thus, in our design we assume an outer layer of 10 cm-thick borated plastic for the CPS. In order to demonstrate how well the shielding design has been optimized, Figure 16 shows a comparison between the prompt radiation dose rates with the optimized shielding design (right) and with 10 cm less tungsten shielding and no borated plastic (left). (Note that in these panels the CPS magnet is assumed to be at the center of the beam line, in contrast with earlier figures.)

C Prompt Dose Rates at the Boundary

In benchmark calculations assuming spheres of pure shielding materials (see a more extensive description of the benchmark calculations in Appendix 2) we find that the prompt dose rate estimates at the RBM-3 boundary are 0.24 μrem/hr for a 3 meter diameter iron sphere and 2.4 μrem/hr for a 1.5 meter diameter tungsten sphere. The baseline design for CPS shielding is assumed to be 85 cm thick tungsten surrounded by 10 cm of borated plastic. Hence, the boundary dose is **below the 2.4 μrem/hr that corresponds to a typical experimental run at Jefferson Lab, for which additional local shielding is not required**. If required, further reductions in the boundary dose can be achieved by optimizing the baseline design in terms of material

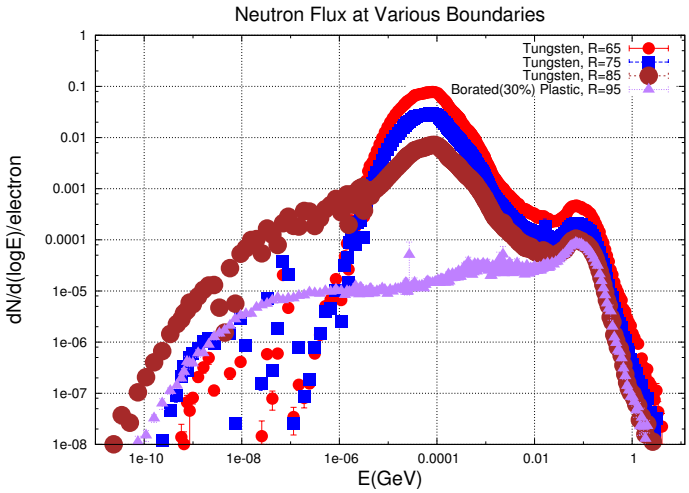

Figure 15. Neutron flux for different shielding configurationsB.

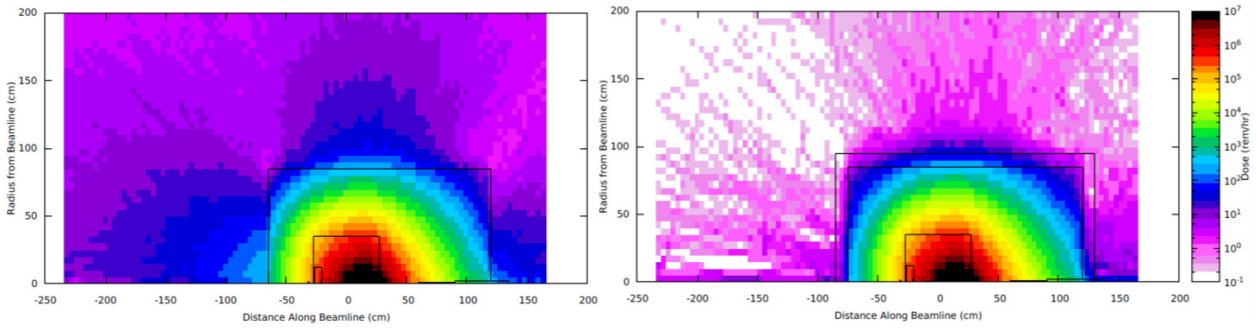

Figure 16. The prompt radiation rates with the optimized shielding design, whereas in the left panel we show the same prompt radiation rates without extra shielding (10 cm less of tungsten shielding, and no borated plastic). Note: these are with the CPS magnet centered around "zero" along the beam line.

choice and geometry. Note also that for Hall D, the CPS design is compatible with the site boundary limits as the standard Hall D tagger magnet can dump up to 60 kW in a local beam dump. Indeed, the Hall D tagger building has been designed assuming a 12 GeV electron beam up to a current of 5 μA. For the CPS, one can thus assume the Hall D tagger magnet building shielding is appropriate in the case for up to 60 kW being dumped in the CPS itself, albeit with the possibility that additional local shielding may be required.

D Activation Dose without a Target

We now turn to the activation dose expected around the CPS following beam-on conditions. Figure 17 shows the calculated activation dose one hour after a 1000-hour experiment has been completed with the same conditions as before (2.7 μA, 10% copper radiator, with shielded CPS). The radiation calculations show the activation dose outside

the CPS is reduced to the order of roughly 1 mrem/hr. To quantify this further, Figure 18 shows the activation dose radially away from the CPS. The activation dose outside the CPS is reduced to 2 mrem/hr at the surface and reduces radially outward. At one-foot distance, it is reduced to about 1.5 mrem/hr, while at two-feet distance it is further reduced to less than 1 mrem/hr. Hence, this demonstrates that the current design meets the requirement that **activation dose outside the device envelope at one foot distance is $\leq$ several mrem/h after one hour following the end of a 1000 hour run**.

Note that these estimates do not depend much on the assumed 1000-hour continuous running assumption, as similar dose rates are seen in a calculation for a 100-hour continuous run, reflecting that much of the activation is instant. Furthermore, activation dose rates do not drop appreciably after one hour or even one day. On the other hand, after one month the activation dose rates at the CPS surface will be reduced by up to a factor of ten. Inside the CPS the activation dose rate can be up to 1 krem/hr, which is why the CPS will be moved laterally to the side after an experiment rather than disassembled.

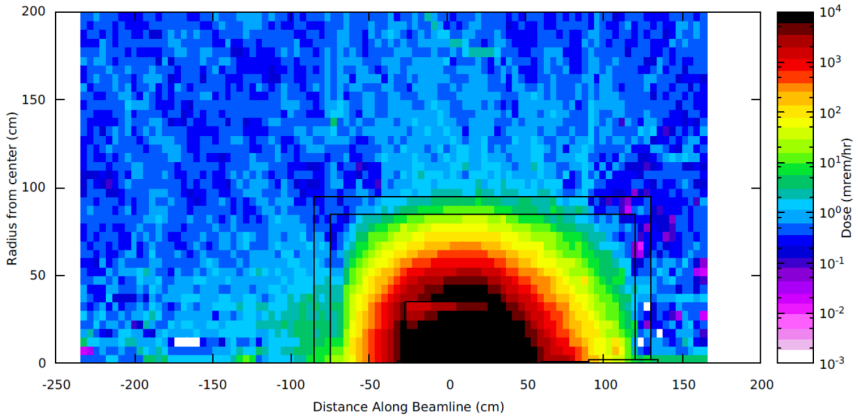

Figure 17. Calculated activation dose one hour after a 1000-hour experiment under the described conditions (2.7 μA, 10% Cu radiator, with shielded CPS) has been completed. Note: these are with the CPS magnet centered around "zero" along the beam line.

E Radiation Dose Rates with a Target

In building further on our radiation calculations, we have included the polarized target scattering chamber and target system. In Figure 19 we illustrate our setup and show a side-view of the CPS, indicating the magnet, the tungsten-powder shield, the layer of borated plastic, and also the scattering chamber with polarized target system. The description of the scattering chamber and polarized target includes: the exact diameter of the scattering chamber and all the ports with accurate dimensions and window materials; and the polarized target material including the liquid helium surrounding the target beads.

Figure 20 is included here for completeness. It illustrates the 1-MeV neutron equivalent damage to silicon (in neutrons/cm^2), which is the relevant quantity to quantify the risk of radiation damage to sensitive electronics. The result, not surprisingly, shows that

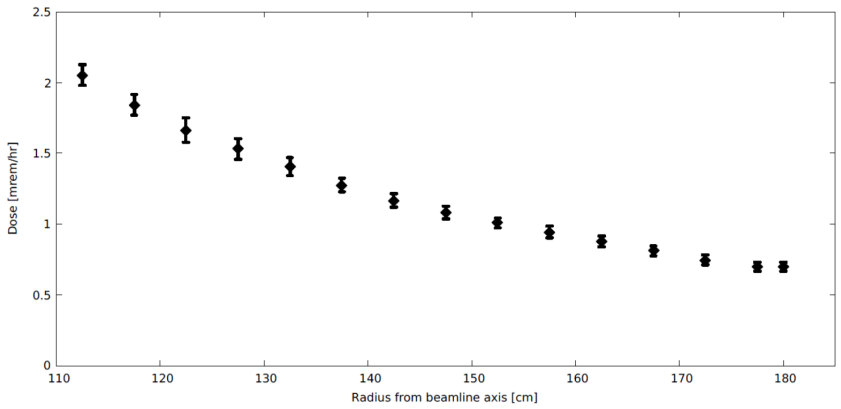

Figure 18. Activation dose outside CPS 1 hour after a 1000 hour run is 2 mr/hr on contact and reduced radially outwards.

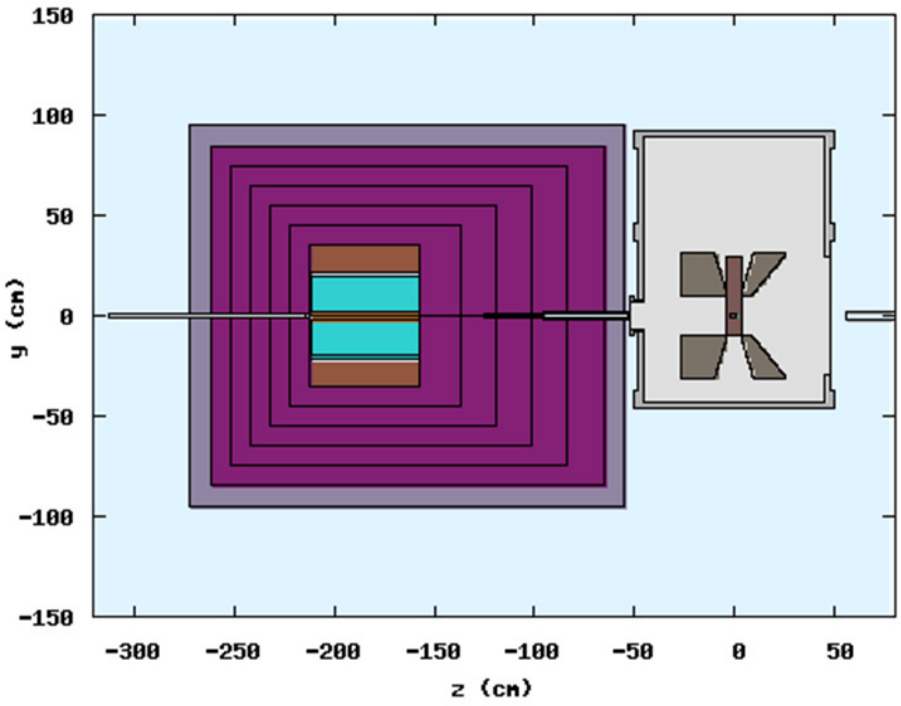

Figure 19. Side view of the Compact Photon Source, indicating the magnet, the W powder shield, and the layer of borated plastic, and also the scattering chamber with polarized target system.

there is a narrow cone in the forward direction, along the beam axis, up to roughly one meter, in which sensitive electronics should not be placed if at all possible.

Figure 21 shows the prompt dose at the target for different configurations. The distance R is radial distance from the pivot, with the radius of the scattering chamber boundary at 50 cm. The various colors on the figure represent the various types of configurations studied: the *100 nA electron beam* (red downward triangles), the *2.7* μA

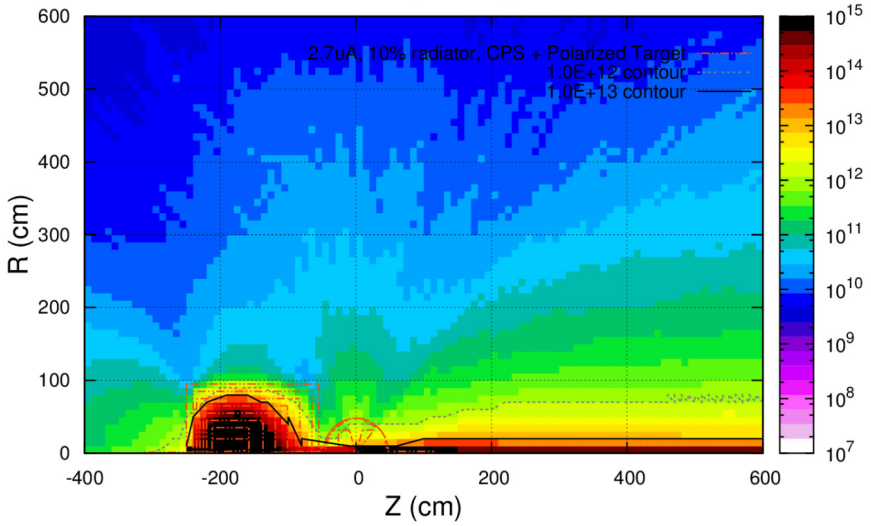

Figure 20. 1-MeV neutron equivalent damage to silicon (in neutrons/cm^2).

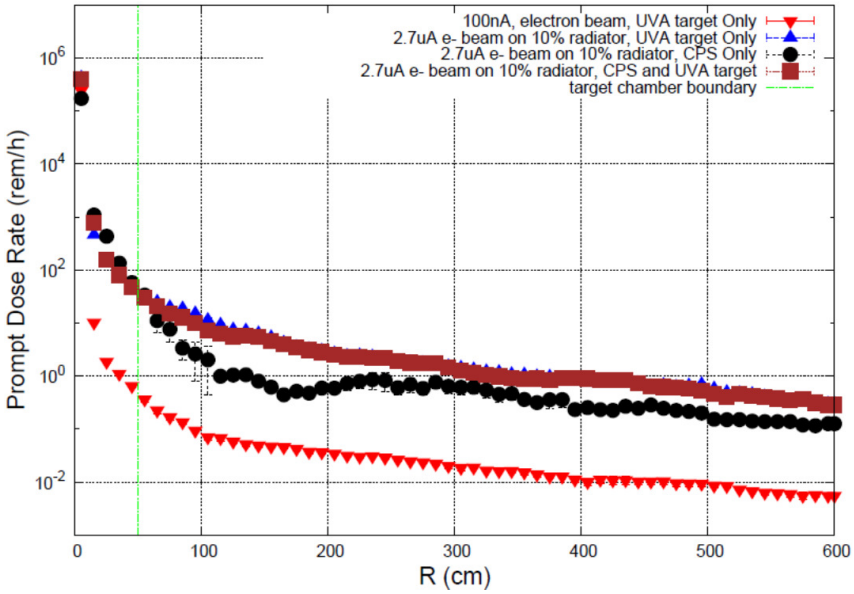

Figure 21. Prompt dose at the target for different configurations. Distance R is radial distance from the pivot, with the radius of the scattering chamber boundary at 50 cm.

photon beam (blue upward triangles), the *CPS without polarized target* (black circles), and the *CPS with polarized target* (mauve squares). At the boundary of the scattering chamber in the *100 nA electron beam* configuration, the default operating mode for polarized beam experiments with dynamically nuclear polarized targets in Hall C to date, the prompt dose is roughly 1 rem/hr. In the *2.7 μA photon beam* scenario it is roughly 30 rem/hr, which simply reflects the fact that even if a 2.7 μA pure photon beam deposits the same heat load in a target as a 100 nA electron beam, the radiation rate is much higher. The *CPS with polarized target* scenario is identical to the pure photon beam case, further

demonstrating that no additional radiation comes from the CPS.

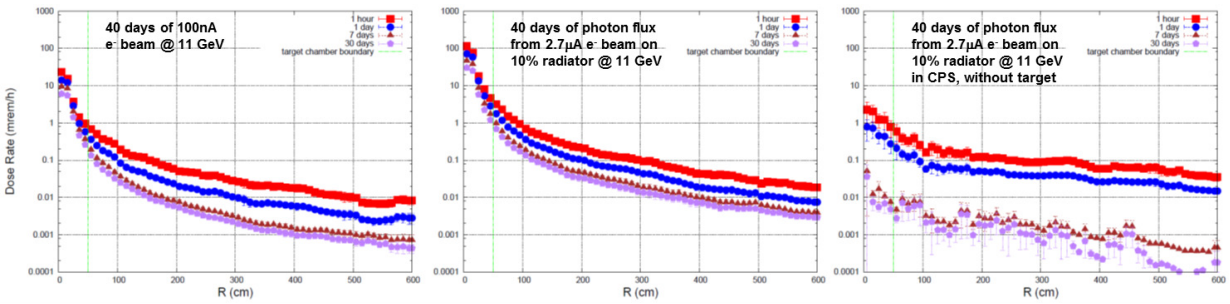

Figure 22. Activation dose rates at the target for different configurations. Distance R is radial distance from the pivot, with the radius of the scattering chamber boundary at 50 cm.

Figure 22 is perhaps more instructive, in that it shows the activation dose rates for the same three configurations. The vertical size of the figure panels have been adjusted such that equal dose rates line up from left to right. One directly can see therefore that the *2.7 μA photon beam* configuration has a much higher activation dose rate than the *100 nA electron beam* case. This again reflects what was seen in the previous figure for the prompt radiation dose rate, as there are many more photons coming from a 2.7 μA electron beam on a 10% copper radiator than there are from a 100 nA electron beam on a roughly 3% dynamically nuclear polarized target. More interestingly, the effect of the CPS is again negligible: activation near the target does not come from the CPS itself, but rather from the photon beam we have created. The price to pay is that one ends up with a roughly constant 0.1 mrem/hr activation level at large radial distances, but this is manageable.

We also indicate in the various panels of Figure 22 how quickly the activation rates drop (after one hour, one day, one week, and one month). One can see that much of the 0.1 mem/hr activation level induced by the deployment of the CPS has decayed away after a week. This is consistent with what was observed in the example of the activation levels at radial distances around the CPS above.

Lastly, we illustrate in Figure 23 in a two-dimensional plot the activation dose rates one hour after a 1000 hour run with the CPS, a 2.7 μA, 11 GeV beam on a 10% radiator and the polarized target system (at z = 0). The 1 mrem/hour contour is indicated. This demonstrates that with the current CPS baseline design, the **activation dose at the pivot in the experimental target area, where operational maintenance tasks may be required, is dominated by the dose induced by a pure photon beam and is at one-foot distance from the scattering chamber $\leq$ several mrem/hr one hour after a 1000 hour run**, and also that **the additional dose induced by radiation of the main beam absorbed in the CPS is negligible**. These were the last of the radiation requirements that were introduced in section IV.

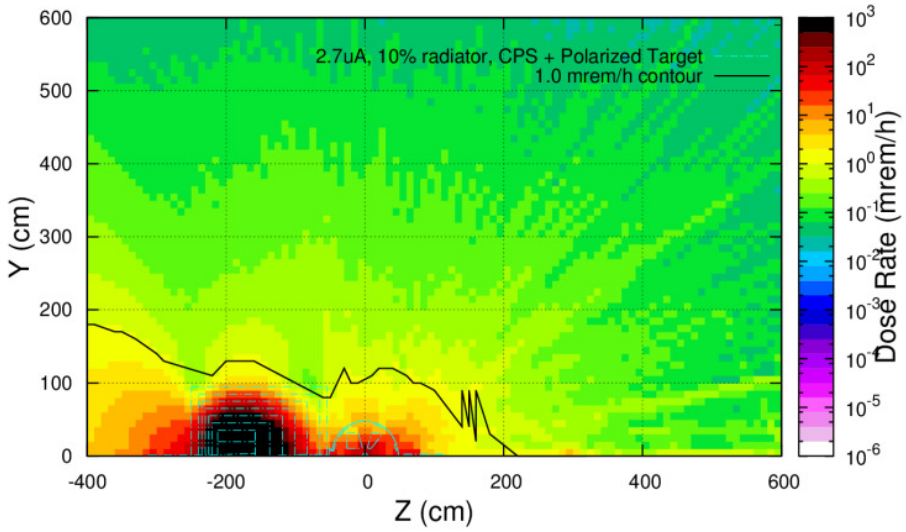

Figure 23. Activation dose rates one hour after a 1000 hour run with the Compact Photon Source, a 2.7 μA beam and a 10% radiator, at 11 GeV beam energy, and the polarized target system (at $z = 0$). The 1 mr/hr contour is indicated. Note that these activation dose rates do not depend much on the assumed 1000-hour continuous run, the rates would be only slightly lower (by 5-10%) and near-identical for a 100-hour continuous run, after one hour.

VI Engineering and Safety Aspects

In this section we will describe the engineering and safety aspects of the CPS. We will start with a summary of material considerations taking into account the high radiation and power inside the CPS, folding in further insights of the radiation studies as relevant for materials for the CPS and the dynamically nuclear polarized target. Then we describe various engineering aspects such as cooling and magnetic forces, and further considerations for assembly and installation of the CPS. We will also outline safety aspects related to the CPS, such as interlocks and fast raster operation during CPS experiments, and post-experiment removal. Lastly, we will give a cost estimate.

A Material Considerations

The level of radiation of the CPS experiments is well below what is typical for many high-luminosity experiments in Halls A and C using regular cryogenics target systems and/or radiators. The prompt radiation level on the polarized target is higher than before, which is simply an artefact of the higher photon flux associated with the higher figure-of-merit of the CPS experiments. The radiation level on the polarized target coils, due to the interaction of the photon beam with the polarized target material, amounts to about 500 rem/hr as illustrated in Figure 24. The radiation levels in the CPS magnet coils, at a distance of 20 cm from the radiation source, are reduced to below 1 Mrem/hr (see *e.g.* Figure 14, bottom right), and allow the use of a modest-cost Kapton tape-based

insulation of the coils [5].

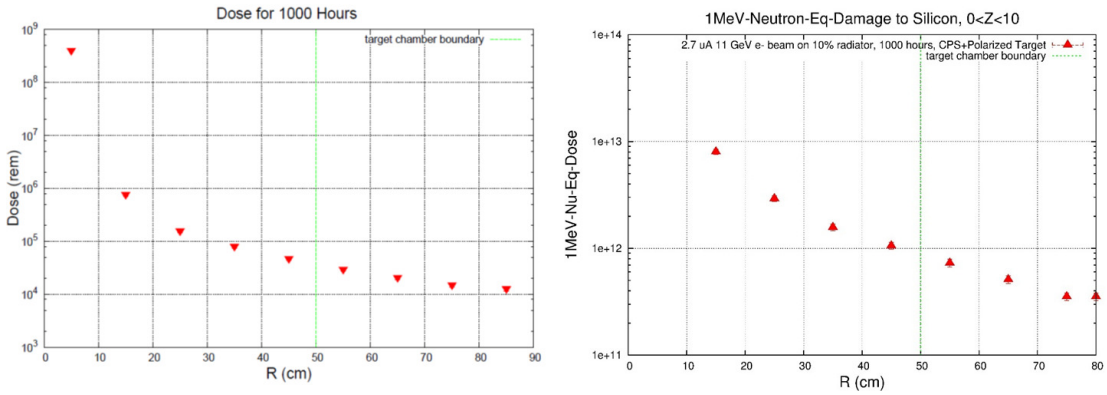

Figure 24. The prompt dose rates (right) and the resulting 1 MeV neutron equivalent damage to silicon (left) in the target area, assuming a 1000 hour run with the Compact Photon Source with a 2.7 mA beam, a 10% Cu radiator, and 11 GeV beam energy. The polarized target system is at z = 0 and the nominal target chamber radius is 50 cm. The target coils are at about 20 cm from the beam line. The dose for 1000 hours of beam time at the target coils is 5 times 10^5 rem and the 1 MeV neutron equivalent damage is 5 times 10^{12} neutrons/cm^2. The contribution of the CPS backgrounds to these numbers is negligible (contributing 2.5% only).

As described in Section III B, we explicitly added a small insert of copper within the tungsten-powder shielding of CPS to act as the beam power absorber. The combination of a small ± 1 mm vertical raster and the magnet field shaping spreads the beam power density over a large surface, such that the temperature of the copper absorber was less than 400°C. This is well below its melting temperature of 1,085°C.

B Cooling and Magnetic Forces

Cooling of the core requires 4 gallons per minute at 110 psi pressure. This will result in a 30°C temperature rise of the cooling water. These values are consistent with provisions in Hall C. Activation of the cooling water of the CPS magnet and beam dump is likely and a closed-cycle cooling system is planned. Hall C has had secondary in-Hall water-cooled dumps of comparable power before, for polarized target experiments in the 6-GeV era. High-power radiators are also not new and have been used with tens of μA on 10% radiation length targets, also with closed-loop water cooling systems. The magnet heat and dump heat can be removed through a heat exchanger to either the Hall C air or LCW. Any activation of the CPS will be confined to a very small volume and in the event of a leak external contamination will be minimized. A leak pan under the CPS could easily be included to catch and confine any leakage up to and including a total loss of primary coolant. A modular pallet mounted design would be efficient and would include primary coolant pumps, DI resin beds, heat exchanger, surge tank, controls, and instrumentation and manifolds.

The CPS magnet will be located relatively close to the 5 Tesla solenoid of the polarized target whose mutual forces need to be taken into account in the design of

the support structure and may require compensation. Preliminary analysis was already performed in the technical note in 2015 for iron-based shielding. In the design the iron-based shielding is replaced by the more effective tungsten-powder shielding, which also much reduced the forces. Residual fields and forces from the CPS magnet will require iron shielding to avoid interference with the Polarized Target magnet.

Another magnetic consideration is the effect on field quality at the polarized target. The fields and gradients imposed on the polarized target will not be large but they must be compensated at the 10^{-4} level. Some further magneto-static effort to model the target environment and design a compensation system is required.

C Assembly and Installation Plan

The CPS should be completely pre-assembled before installation. The pre-assembly can be done in the Hall or more likely in the Test Lab High Bay, or equivalent area. The outer dimension of the CPS tungsten-powder shielding as outlined for optimized shielding (see Figure 16, right panel) is 1.7 m by 1.7 m by 1.95 m, or a volume of 5.63 m^3. From this, one needs to subtract the inner box including the magnet, which amounts to 0.26 m^3. This means a net volume of 5.37 m^3, or 88 tons, for the optimized tungsten-powder shielding presented. In total, the CPS weight is estimated to be 100 tons. Hence, a reinforced floor is required for CPS assembly, as exists in both the Test Lab High Bay and the Hall itself. Note that if one would reduce the overall size of the W-powder shielding by 5 cm on each side, it would imply an increase of the radiation levels by about 50%, and a reduction to 4.48 m^3 or 73 tons (for the W-powder). If one would remove an additional 10 cm only on the bottom side, towards the floor, for an additional factor of two increase in radiation level in the direction of the floor, this reduces to 68 tons.

Alternatively, we could round the W-powder box corners, as illustrated in Figure 25. This would complicate modular construction, but would allow to reach similar radiation levels aas with the optimized design, while reducing material needs and weight. To verify this, we updated the FLUKA model originally developed by one of us (Parker Reid (SMU)) for this report, and by replacing the W-powder ($\rho = 16.3\, g/cm^3$) with B(5%)-CH_2 in the rounded corners. The result of the FLUKA analysis confirmd that such a configuration has the same level of radiation outside of the CPS as the optimized shielding design model, but with the volume (and weight) of the W-powder reduced by 25%, to $\circ$66 tons.

During assembly and after completion the CPS can be measured and fiducialized to facilitate final alignment in Hall C. Progressive measurement and fiducialization will eliminate problems with position references becoming hidden. Transporting the CPS to (or within) Hall C in one piece will preserve the alignment and avoids introduction of errors due to dis-assembly and re-assembly. This would require a large crane in Hall C, similar as for examples was used for G0 installation and removal, and for SOS removal.

The CPS will be installed in the area upstream of the Hall C pivot (see Figure 26). The polarized target chamber will be installed instead of the regular scattering chamber, and the CPS will be installed replacing the final Hall C beam line girder and one horizontal bend magnet, the most downstream magnet of the 12-GeV Hall C beam line. The final Hall C beam line girder (Figure 27) contains the beam position diagnostics for the regular Hall C electron scattering experiments, including a double set of superharp and beam

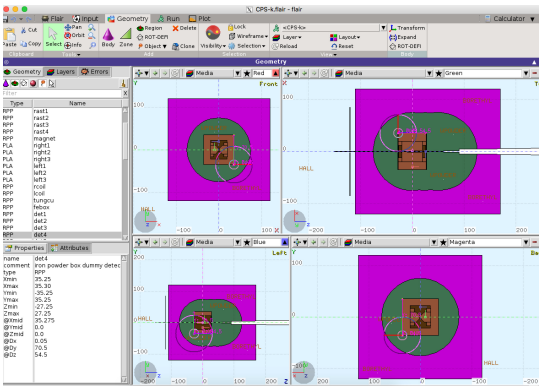

Figure 25. The FLUKA model used in calculations of radiation. Here, front, back, right and left views are shown, illustrating the rounded W-powder (green) corners and the outer borated plastic (purple) volume.

position monitoring systems. These are used to define the incident beam position and beam angle, but not needed for the CPS experiments (where we rather need to know the beam position on the radiator). The horizontal bend magnet, the most downstream (blue) magnet on Figure 28 was installed as precaution to prevent beam steering of the SHMS at small angles. This magnet is not required, especially as the foreseen CPS experiments used ancillary detector systems such as NPS and BigBite. Instead of this magnet, a small girder with one beam position monitor and superharp system is foreseen, to define the electron beam-radiator interaction point.

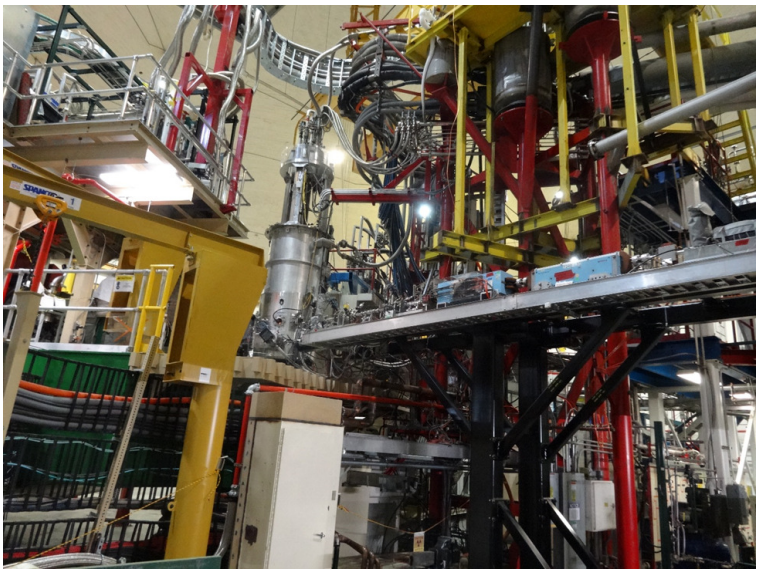

Figure 26. Final Hall C girder, SHMS data cable conduits and environment.

The downstream portion of the last beam line girder is cantilevered over the SHMS data cable hoses which arc around the pivot and permit rotation. The SHMS cable conduits cannot be removed or significantly modified. They do permit legs for the CPS stand, but they may limit the rotation of the SHMS somewhat. A platform for the

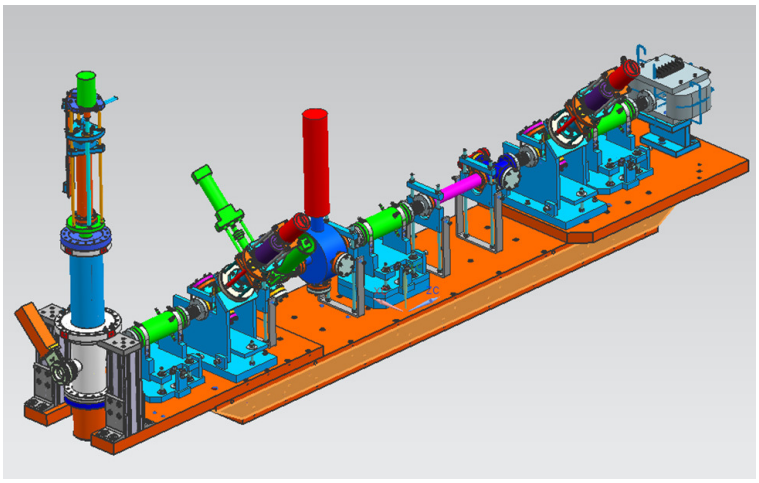

Figure 27. The present final girder in Hall C.

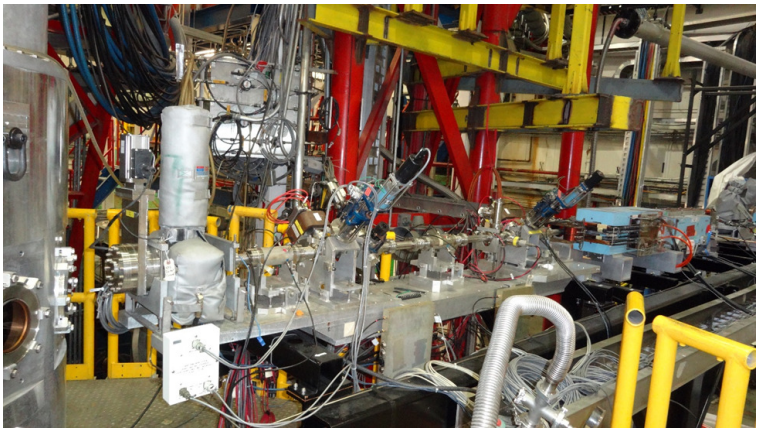

Figure 28. Closer view on final Hall C girder.

CPS could perhaps be welded and bolted from the top of the pivot cylinder (under the scattering chambers) to an upstream stand. The addition of CPS stands and/or a welded platform still requires further design and engineering. We do note that one support leg of a platform (the lowest yellow support bar on Figs. 26 and Figure 28) will need to be moved, but this can be done.

Installation in Hall C will consist of the following steps:

- Removal of the final beam line girder
- Removal of the horizontal bend magnet
- Presurvey and mount of CPS stand to Hall C floor
- Transport and crane in complete CPS using a larger than 100 ton truck crane
- Survey and alignment of CPS
- Installation of new small beam girder and instrumentation (upstream of CPS)

- Survey and alignment of new girder
- Connect CPS magnet power and water and test
- Connect new girder and test
- Restore beam vacuum in Hall C
- CPS hot checkout

D Equipment Safety and Interlocks

Whereas the closed-loop cooling requirements of the CPS in themselves are not new to Hall C, the combination of a high-power radiator, magnet and beam dump inside a shielded box impose reliability and remote handling considerations. The primary engineering controls providing personnel protection are to make the design as robust as possible, with large safety margins, and evade disassembly for maintenance and repair, or equipment removal, altogether.

The CPS should be heavily instrumented for early detection of problems such as low coolant flow, leaks, low pressure, high temperature, and high conductivity. The protection and safety of the CPS begins with the design which must err on the side of conservatism especially in the magnet coil design and dump cooling. A low current density design is envisioned, not to exceed 500 Amps/cm^2. Individual coil pancakes leads should be extended to an area outside of the magnet and shielding for easy access. There should be NO electrical or coolant joints inside the CPS shielding. Every separate sub coil of the CPS magnet should have thermometry, klixons and flow measurements to avoid any possibility that one of the separate current paths can overheat due to lack of sufficient coolant, a leak or a bad electrical joint. Voltage monitoring of each sub coil should insure against overheating from any source including internal blockage, leaks, flow restrictions or bad electrical connections. Extra insulation between sub coils and between the coil and ground should be added to prevent ground faults. Lastly, a commercial power supply is assumed and these come with a wide array of internal interlock protections. The available interlocks and signals would be fed into the FSD system.

To protect equipment during CPS operations, a dual protection scheme is suggested using both the Hall C BPM system and direct instrumentation of the fast raster magnet itself. The BCMs would monitor beam position and motion in close to real time and coil voltage monitoring on the raster coils would provide ample early warning of raster problems. Both these independent signals would be fed into the FSD system. Radiator temperature could be monitored to provide a third independent protection system, and if implemented, thermocouples mounted on the radiator should be robust against radiation damage and provide fast enough protection against radiator overheating. Simulations of various magnet failure modes such as reduced or no water flow, overheating, etc., can be used to proof test instrumentation and interlocks. These tests would be performed in Hall C after final installation as part of the usual hot checkout procedures.

E Post-Experiment Removal Plan

The CPS is expected to become activated and contaminated by the completion of the experiment. Activation levels inside the CPS are expected to be and remain high, until well after experiment completion. Exposure to Hall C staff will be minimized by designing the CPS for a one-piece removal. The total weight of the CPS is about 100 tons, too heavy for the Hall C crane so this will require use of a large truck crane. The CPS will then be stored on the periphery inside Hall C, most likely at the location where the beam either enters or exits the Hall boundary, under the beam line. This eliminates the need for staff to dis-assemble the CPS.

Water disconnects using self-sealing connectors can be used to eliminate any primary cooling water loss. The DC Power supply and air-cooled cables will be disconnected and removed as they are not expected to be activated. The cooling water pumps, controls, DI resin beds and heat exchanger will likely have contaminated water inside but will not otherwise be activated. The cooling pallet can be removed to storage intact or the water drained and stored separately or disposed of. The radiator infrastructure can be stored as with other Hall C experiments using radiators. After the CPS removal, the small girder removal, and the CPS stand removal, the regular last beam line girder and horizontal pre-bend magnet can be installed and surveyed in their locations again, to restore the default 12-GeV Hall C electron beam line.

F Initial Cost Analysis

A preliminary cost analysis has been made. The W-powder and magnet costs are based on a vendor quotation and estimate, other items are engineering estimates. The CPS cost will be dominated by the cost of W-powder. Here, we assumed the cost for the optimized shielding design, requiring 88 tons. We could reduce with roughly 25% if rounding the W-powder box corners (see Figure 25) proves feasible, or we could reduce the size of the W-powder box with about 20% at the expense of increasing the radiation levels by up to a factor of two, or potentially even consider both.

- Tungsten powder shield, 88 tons - $3300K
- CPS Magnet, includes mechanical design and tooling - $98K
- Copper core absorber and closed loop water cooler - $25K
- W-Cu (20%) insert, 1 ton - $100K
- Borated plastic outer layer - $100K
- Support structure and elevation jacks - $50K
- Beam line: Radiator system and raster magnet with power supply - $50K
- Beam line: small girder with superharp and BPM - $50K
- Closed-loop magnet and dump cooling system -$25K

- Instrumentation, controls, and interlocks - $50K
- Rented crane and crew - $10K/day

The total cost estimate amounts to nearly $4M, with the tungsten-powder as the dominant part. The reduction of tungsten powder, with 25% if rounded coreners prove feasible, and potentially more at the expense of slightly increased radiation levels, can act as contingency. Alternatively, one could consider use of surplus lead as a cheaper shielding material option, but this would roughly double the CPS weight.

VII Acknowledgements

We thank Paul Brindza for helpful discussions and providing valuable input for the writing of this document.

---

[1] D. Keller, "The UVa approved and proposed experiments", in arXiv:1704.00816.

[2] B. Wojtsekhowski and G. Niculescu, "Conceptual Design Report, A Compact Photon Source", Supplementary material for the WACS proposal PR12-15-003 to the JLab PAC 43, June 2015; in arXiv:1704.00816.

[3] D. Hamilton, "Photon Beam Requirements for Wide-Angle Compton Scattering", in arXiv:1704.00816.

[4] P.K. Kloeppel, "Design for 25-kW beam dumps at 100 MeV and 500 MeV", CEBAF-TN-90-205; M. Wiseman, C.K. Sinclair, R. Whitney, M. Zarecky, "High Power Electron Beam Dumps at CEBAF".

[5] V.V. Petrov, Yu.A. Pupkov, a report "BINP TESTING OF RADIATION RESISTANCE OF THE MATERIALS USED FOR PRODUCTION OF ACCELERATOR MAGNETIC SYSTEMS", Novosibirsk, 2011

Appendix 1: Concept Transfer to Hall D

The intense photon source is one component of the K_L beam. The experimental method can be summarized as follows: electrons hit a copper radiator, the resulting photons hit a Be target, and a beam to K_L is produced. The search for missing hyperons is a strong motivation for this setup.

The new setup utilizes the Hall D Tagger vault, properly shielded by design to accomodate the medium power beam dump capable of accepting up to 60 kW of 12 GeV electron beam, assuming that proper local shielding is set around the dump. The presently installed dump is placed behind the iron labyrinth walls, and is surrounded by a massive iron shielding, made of iron blocks available at the time of construction. The standard GlueX setup is optimized for operations using very thin radiators producing relatively low intensity photon beam such that the beam electrons losing energy to photon production in

the radiator may be detected and counted in the tagger hodoscope counters. The present setup is not suitable for production of massively more intense photon beams needed for the K_L production, due to the expected overwhelming radiation and activation levels in the vault.

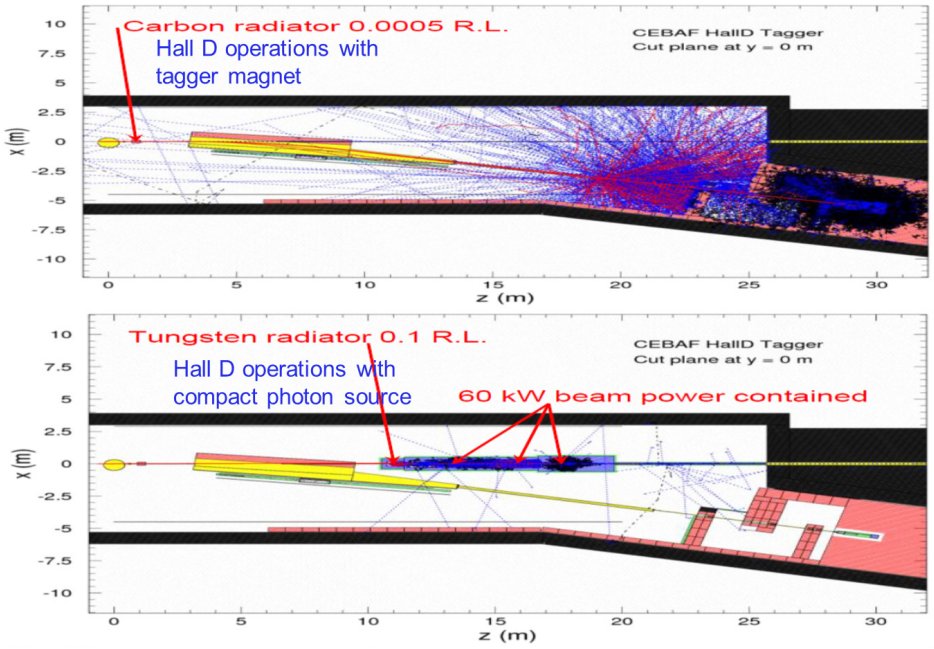

Figure 29. 2D projection of backgrounds in the Hall D alcove for both, the nominal GlueX beam/dump and the 5μA/CPS configuration.

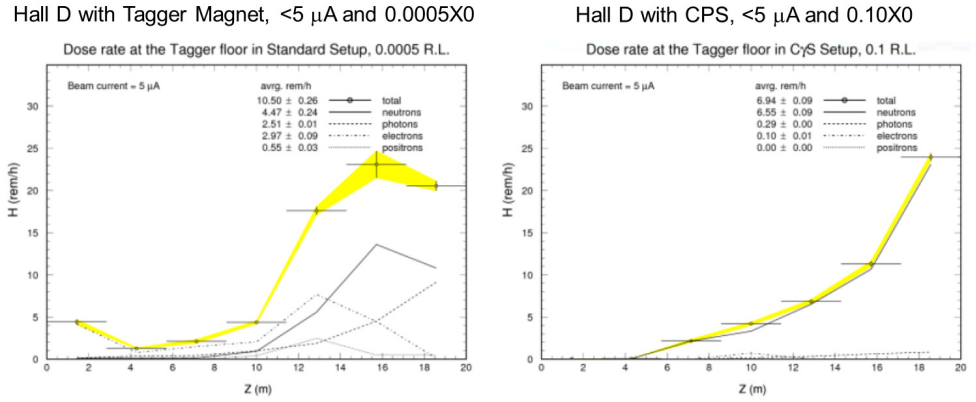

Figure 30. Dose rate at the tagger in standard configuration (left) and with CPS and 10% radiator (right). The CPS with its optimized shielding design does not increase radiation levels beyond standard configuration.

The CPS will be located downstream of the tagger magnet. The tagger alcove has more space than that available in Hall A/C, so positioning and shielding placement are simpler. Indeed, the CPS implementation in Hall D may have a different length and

magnet field, as well as shielding. A total floor loading of the implementation up to 100t is acceptable. If one uses a 2nd raster system for Hall D to compensate for the initial 1mm rater, this can be an equivalent essential design to the Hall C/A one.

As discussed in section IV, the Compact Photon Source converts beam energies of up to 12 GeV with currents of up to 5 μA into a high-intensity source of collimated photons. For the Hall-D adaptation, the 5 μA beam current is limited by the design of the Hall D Tagger Magnet alcove. This corresponds to a 60 kW power limit. Note that the ceiling shielding of the Tagger hall above the CPS position is the same as it is above the existing 60 kW dump. No radiation increase at the site boundary is thus expected with respect to 60 kW operations using the existing dump. Figs. 29 and Figure 30 illustrate how the CPS stops the electron beam and absorbs almost all beam energy inside, and therefore provides excellent shielding. Running the CPS at full beam power produces radiation fields in the Hall D tagger area, comparable with running regular Hall D experiment utilizing a very thin radiator in front of the tagger magnet.

Appendix 2: Benchmark comparison

From the engineering standpoint, two of the most important aspects in the design and subsequent building of a Compact Photon Source are the ability to properly shield the radiation produced inside the source and to dissipate the resulting heat in a safe manner. While the latter point was addressed earlier in this document, in this Appendix we focus on the former issue, specifically detailing the steps taken to benchmark the simulations used in assessing the prompt, as well as the residual (activation) radiation level around the CPS and in the experimental Hall. Even though they have been mentioned before, it is worth reiterating the basic radiation level constraints associated with experiments at JLab:

From the radiological protection point of view the following set of limitations should be satisfied, conservatively assuming typical expected experimental run conditions:

- Beam energy: 11.5 GeV Beam electron beam
- Current: 2.6 μA
- Beam Power (based on the above) = 30 kW
- Run time: $\sim$ 1000 hours

For the typical, high current JLab experiment the radiation dose rate parameters must stay within the following limits:

- Dose rates in the Hall should be under several rem/h at 10 m from the device
- Dose rates at the boundary should be under 1 $\mu rem/h$ during the run
- Dose rates outside the device envelope at a foot distance from the device should be under several $mrem/h$ after one hour following the end of the 1000 hour run

In order to gain an understanding of the radiation levels likely to be produced by the CPS and to ultimately design the optimal shielding for it, one relies on Monte Carlo simulations and over the years the nuclear and particle physics community[1] has developed a series of very sophisticated simulation programs. In time these programs became more complex, with several physical processes that can be turned on and off, various thresholds and cutoffs that might greatly influence the result yet they are buried deep inside the code. Therefore, one has to be careful in using and interpreting the results of such simulations because, as suggested above, the same simulation can give vastly (i.e. orders of magnitude differences) different results with only (seemingly) minor changes in the input parameters.

Ideally one would want to **ground–truth** the simulation by **experimentally measuring** a small but relevant setup and verify that the simulation results agree with the measured radiation levels of that setup. For the current study this step was not done explicitly, though one can argue that one of the simulation programs used (Geant3) was extensively **ground–thruth–ed** as the JLab RadCon group compares the radiation levels measured at boundary of the experimental Halls with the Geant3 predictions.

To benchmark the simulations used in the CPS design a couple of relatively simple radiation scenarios were independently simulated using three different simulation programs (Geant3[2], Fluka[3], and Geant4[4]) by the three groups involved in this process, as follows:

- JLab group (led by P.D.): used Geant3
- UVa group (led by J.Z.): used Fluka
- JMU group (led by G.N.): used both Geant4 and Fluka

The geometry that was simulated was a simple sphere with a small cylindrical hole bored in it such that the 30 kW, 11.5 GeV beam interacts inside the sphere (at $z = 30$ cm for the Fe sphere and at $z = -15$ cm for the W sphere).

---

[1] As well as related areas such as nuclear medicine, astronomy, defense, etc.

[2] The only code currently setup for calculating the radiation at the JLab boundary is Geant3.

[3] Fluka is the only choice for activation calculations.

[4] The development of the Fortran–based Geant3 code has ceased long time ago and the community has/is migrating toward the C++ based Geant4.

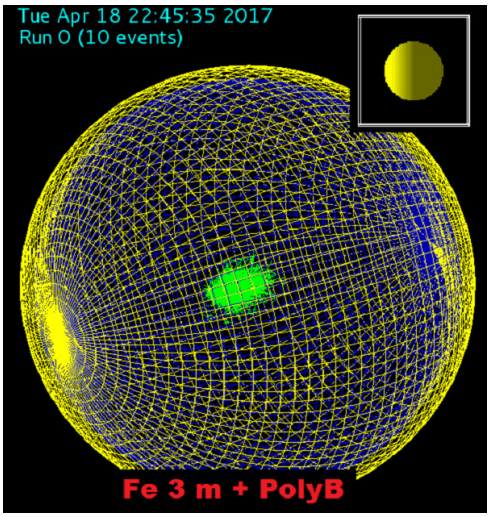

Figure 31. Fe sphere with the Borated Poly layer, as simulated in Geant 4.

Four of these setups were simulated:

- A 300 cm diameter **Fe** sphere
- A 150 cm diameter **W** sphere
- A 300 cm diameter **Fe** sphere with an outer 10 cm Borated Polyethylene layer (5 % Boron by weight
- A 150 cm diameter **W** sphere with an outer 10 cm Borated Poly layer

The results of these parallel simulations are summarized in the Table below.

	Dose Rates [mrem/h]								
	JLab DINREG/Geant3			JMU Geant4			UVa Fluka		
	n	γ	total	n	γ	total	n	γ	total
3 m Fe	146	0.44	146.44	123.2	0.56	123.76	10	0.039	10.039
3 m Fe + Poly- B	0.8	2.8	3.6	0.284	0.56	0.844	0.11	0.063	0.173
1.5 m W	13	0.06	13.1	6.34	0.33	6.67	1.7	0.0002	1.7002
1.5 m W+Poly-B	2.7	0.003	2.7	1.76	1.28	3.04	0.15	0.0007	0.1507

Table I. Geant3, Fluka, and Geant4 prompt radiation comparison for Fe and W spheres.

Examining these results one notes the reasonable agreement between the Geant3 and Geant4 simulation, though factors of 1–2 could not be ruled out in the differences (and are to be expected in these types of estimations). The radiation levels predicted for these spheres leads one to conclude that the optimization of the CPS shielding satisfying the safety requirements in the Halls and outside ought to be possible. The addition of a borated polyethylene layer seems to be absolutely critical in moderating and absorbing low energy neutrons. This becomes very important if one choses[5] Fe as (part of) the shielding material.

One notes that a dose rate of $\sim$2.4 $\mu rem/h$ at the boundary correspond to a "regular" normal experiment, not requiring extra shielding measures, corresponding to about the "200% of allowable design boundary dose rate" (that is, the dose rate at which the dose accumulation would be 10 mrem if such conditions are run for a half of the calendar year continuously).

The Fluka simulation (carried out in parallel at UVa and at JMU) was able to provide residual radiation (due to activation) at various time intervals: 1 hour, 24 hours,

[5] For example for cost containment.

7 days, 30 days. Sample results for the 3 m Fe sphere, one hour after the end of the irradiation cycle (assumed to be 1000 hours of 11.5 GeV, 2.6 μA beam) are shown in the Figures below.

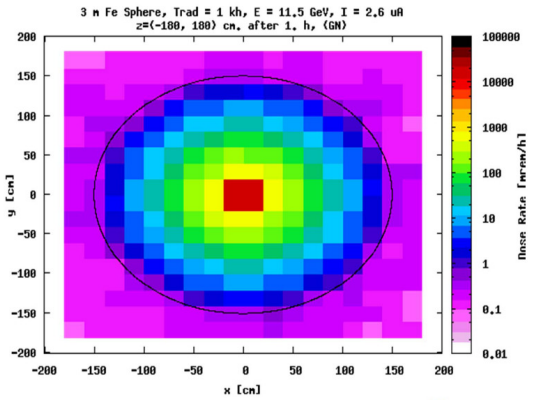

Figure 32. Radiation level one hour after the end of the irradiation period. Closeup view of the JMU Fluka result.

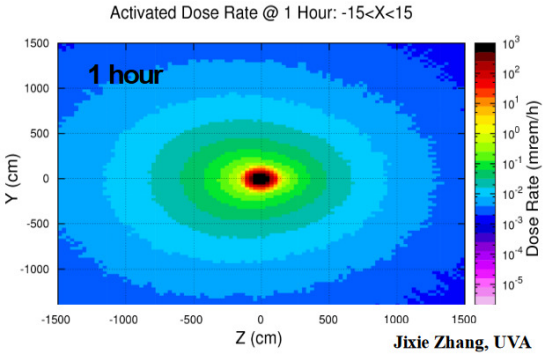

Figure 33. Expanded view of the radiation level one hour after the end of the irradiation period (UVa Fluka result). Both plots correspond to the 3 m Fe sphere.